crystals

MDPI

Article

Quantum-Mechanical Calculations of the Electronic Structure of $Ln_2Zr_2O_7$ Zirconates (Ln = La, Nd, Sm, Eu, and Gd) with the Pyrochlore Structure

Anatoly Lavrentyev [1,*], Boris Gabrelian [2], Tuan Vu Van [3,4] and Kseniia Kalmykova [1]

[1] Department of Electrical Engineering and Electronics, Don State Technical University, Rostov-on-Don 344000, Russia; kfkalmykova@donstu.ru
[2] Department of Computer Software for Computing Machinery and Automated Systems, Don State Technical University, Rostov-on-Don 344000, Russia; bgabrelyan@donstu.ru
[3] Division of Computational Physics, Institute for Computational Science, Ton Duc Thang University, Ho Chi Minh City 700000, Vietnam; tuan.vu@vlu.edu.vn
[4] Faculty of Electrical & Electronics Engineering, Ton Duc Thang University, Ho Chi Minh City 700000, Vietnam
* Correspondence: alavrentyev@donstu.ru

Abstract

Five compounds with the formula $Ln_2Zr_2O_7$ (Ln = La, Nd, Sm, Eu, and Gd) were investigated. These materials exhibit important physicochemical properties and find practical applications for the development of high-temperature barriers, gas traps, and the adsorption of actinides in nuclear waste. The investigations were performed using ab initio calculations within the framework of density functional theory employing the full-potential augmented plane-wave method. Quantum-mechanical calculations of the electronic structure and optical spectra of the investigated semiconductors were carried out using the exchange-correlation potential within the generalized gradient approximation (GGA), incorporating GGA + U corrections to account for strong correlations among f- and d-electrons, as well as the GGA + U + mBJ approach to obtain more realistic band gap (E_g) values. Relativistic spin–orbit coupling effects within the electronic systems of heavy-element atoms were also taken into account. The band gaps (E_g) and the complex dielectric function, from which optical properties can be derived, were calculated. A comparison of the calculated total densities of states (DOS) with experimental X-ray photoelectron spectra (XPS) demonstrated the validity of the applied exchange-correlation potential corrections and highlighted the importance of accounting for the spin–orbit splitting of atomic electronic states to accurately reproduce all features of the experimental XPS spectra.

Keywords: pyrochlores; electron-energy structure; density functional theory; exchange-correlation potentials; optical properties

Check for updates

Academic Editor: Dmitri Donetski

Received: 7 September 2026
Revised: 28 September 2026
Accepted: 9 October 2026
Published: 15 October 2026

Copyright: © 2026 by the authors. Licensee MDPI, Basel, Switzerland. This article is an open access article distributed under the terms and conditions of the Creative Commons Attribution (CC BY) license.

1. Introduction

Pyrochlores with the general formula $Ln_2Zr_2O_7$ (Ln = La, Sm, Nd, Eu, and Gd) possess a wide variety of interesting physicochemical properties associated with their low thermal conductivity and high melting temperature, as well as their stability and resistance to defect formation [1–3]. $Ln_2Zr_2O_7$ pyrochlores can be used as thermal insulation for metal components in aviation and marine turbines, as well as in fuel cells as high-temperature ceramic barriers, in gas traps, in metal oxide transistors, and for the immobilization of actinides in nuclear waste [4–8]. The applied nature of pyrochlore research is also related to their use in laser technology and optics.

The general formula of the investigated pyrochlores is $Ln_2^{3+}Zr_2^{4+}O1_6^{2-}O2^{2-}$ (O1 and O2—oxygen atoms in nonequivalent positions), where the metal cations Ln = (La, Sm, Nd, Eu, and Gd) and Zr have valences of 3+ and 4+, respectively [9].

The crystal structure of the $Ln_2Zr_2O_7$ pyrochlores belongs to the Fd-3m space group [10] and can be described as a defect fluorite solid solution, in which the cations form a face-centered cubic (fcc) lattice and 1/8 of the atomic sites are vacant to maintain charge neutrality (the crystal structure is shown in Figure 1).

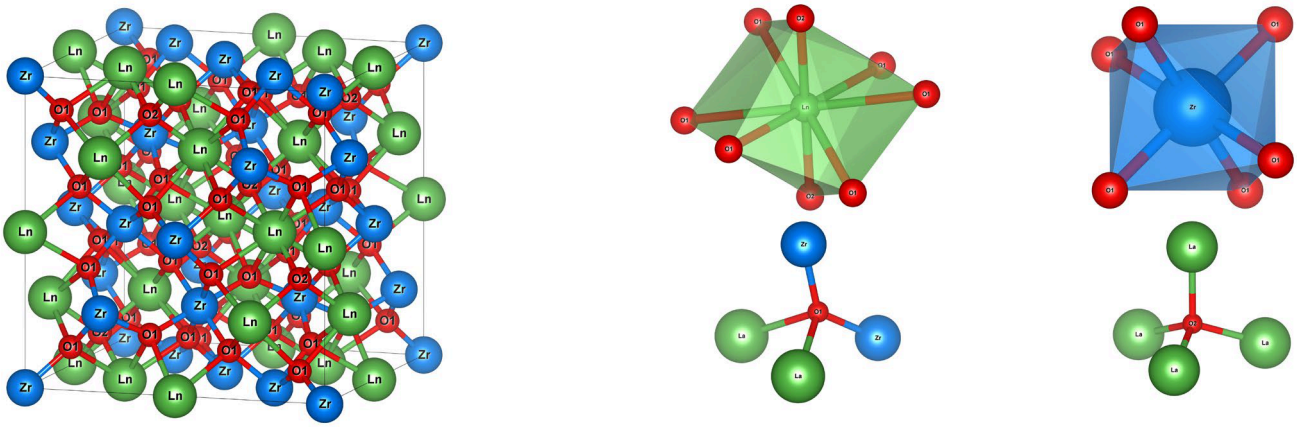


Figure 1. Crystal structure of the pyrochlore and the nearest coordination environment of Ln (La, Nd, Sm, Eu, and Gd), Zr, O1, and O2 atoms.

In the crystal structure of $Ln_2Zr_2O_7$, there are five unique crystallographic positions according to Wyckoff notation: the Ln cations (La, Nd, Sm, Eu, and Gd) occupy the 16d positions, the Zr cations occupy the 16c positions, and finally, the 48f positions are occupied by O1 oxygen atoms, while the 8b positions are occupied by O2 oxygen atoms (Table 1). As noted above, the 8a sites ($\frac{1}{8}$, $\frac{1}{8}$, $\frac{1}{8}$) are completely vacant. The O2 oxygen ions at the 8b sites ($\frac{3}{8}$, $\frac{3}{8}$, $\frac{3}{8}$) are tetrahedrally coordinated by the rare-earth Ln cations (La, Nd, Sm, Eu, and Gd). The O1 oxygen ions in the 48f positions have coordinates (δ, $\frac{1}{8}$, $\frac{1}{8}$); they are displaced toward the adjacent vacant 8a sites and are coordinated by two Ln cations (La, Nd, Sm, Eu, and Gd) and two Zr cations [10]. The rare-earth Ln cations (La, Nd, Sm, Eu, and Gd) are coordinated by six O1 oxygen atoms (48f positions) and two O2 oxygen atoms (8b positions), with the Ln–O2 interatomic distance being shorter than the Ln–O1 distance. The six-coordinate Zr cations are located at equivalent distances from the O1 atoms, forming trigonal antiprisms with $3(D_{3d})$ point symmetry.

Table 1. Atomic basis of the pyrochlore structure; atomic coordinates are given in units of the lattice parameter *a*.

Atom	Wyckoff Position	x	y	z
Ln	16*d*	0.5	0.5	0.5
Zr	16*c*	0	0	0
O1	48*f*	δ	0.125	0.125
O2	8*b*	0.375	0.375	0.375

The crystal structures of all the pyrochlores investigated in the present work are identical; they differ only in their lattice parameters and the displacement values δ of the O1 atom. In this study, the lattice parameter a and the free parameter δ were determined computationally.

Previous calculations of the electronic structure have also been performed for the compounds studied herein [11–14]. However, in Refs. [12–14], the exchange potential included

only the correction for the strong intra-atomic interaction of the rare-earth f-electrons, whereas in Ref. [11], even this correction was omitted. Furthermore, the optimization of the crystal unit cell parameters was not performed in Refs. [13,14]. In Ref. [12], an anomalous step-like variation in the band gap of $Eu_2Zr_2O_7$ was obtained upon increasing the parameter governing the strength of the f-electron interaction, without any discussion of the possible reasons for such behavior.

2. Materials and Methods

The electronic structure calculations were performed within the framework of density functional theory (DFT). The wave functions were expanded using the augmented plane-wave plus local orbital (APW + lo) method, as implemented in the WIEN2k package (version 24.1) [15]. The calculations were carried out in reciprocal space. A uniform k-point mesh was generated within the Brillouin zone, and integrations were subsequently performed over these points. A mesh of 1000 k-points was used for the electronic structure calculations, and a mesh of 5000 k-points was employed for the calculation of the dielectric function.

The computational scheme is all-electron—meaning that all valence and core electrons are treated explicitly at each iteration of the self-consistency procedure—and full-potential, implying that no a priori shape is assumed for the potential, unlike in the muffin-tin approximation.

For sufficiently heavy atoms, spin–orbit interaction becomes significant. Spin–orbit (SO) coupling in WIEN2k is calculated using a second-variational procedure and allows the eigenvectors to be obtained from the scalar-relativistic electron wavefunctions. Details can be found in [15]. For all investigated compounds, spin–orbit interaction was taken into account in the calculations of the crystal potentials.

Various corrections to the exchange-correlation potential were employed in the calculations. First, the generalized gradient approximation (GGA) in the PBE parametrization [16] was used. This approximation is based on mean-field theory, is semilocal, and depends solely on the total spin electron density $\rho_\sigma\left(\vec{r}\right)$ and its gradient $\nabla\rho_\sigma\left(\vec{r}\right)$.

However, the exact exchange potential exhibits a step-like structure, and its derivative with respect to particle number exhibits a discontinuity. To account for this, a second correction (GGA + mBJ) was applied using the semilocal potential proposed in Ref. [17] (the modified Becke–Johnson, or mBJ, potential), which also depends on the kinetic energy density of the occupied states.

Third, the specific behavior of the f-electrons in the rare-earth elements (Nd, Sm, Eu, and Gd) had to be accounted for in this study. To this end, the GGA + U approach [18] was employed, which introduces a Hubbard U correction exclusively for the strongly correlated d- and f-electrons, thereby separating the unoccupied and occupied f-states. A value of U = 5 eV was used for 4f-states of Nd, Sm, Eu, and Gd; 5d-states of La and Gd; and 4d-states of Zr in all calculations. As recommended by the authors of Ref. [15], the effective value U − J was used as U.

The application of these corrections in the electronic structure calculations leads to the opening of a band gap (E_g), whereas within the standard GGA approximation (a mean-field approximation), the band gap (E_g) is absent for $Nd_2Zr_2O_7$, $Sm_2Zr_2O_7$, $Eu_2Zr_2O_7$, and $Gd_2Zr_2O_7$ compounds.

Other corrections can also be applied. There are many studies in which the authors compare the influence of different corrections to the exchange-correlation potential on the electronic structure of various compounds (for example, [19]). Thus, the use of hybrid potentials in model calculations often allows one to obtain band gap (Eg) values for semiconductor compounds that are close to the experimental ones. However, their use leads to

significantly more computationally demanding calculations. The authors of [17] showed in their study that the application of the semi-local mBJ potential, which does not require such high computational costs, yields Eg values just as close to the experimental ones. In the present work, we aimed to explain all the main features of the electronic structure of the investigated zirconates using the minimum necessary number of corrections.

3. Results and Discussion

For all the investigated compounds, the unit cell lattice parameter a was optimized to minimize the total crystal energy. To this end, an initial value of a was chosen to establish a reference unit cell volume, followed by calculations for values corresponding to unit cell volumes 5% and 10% smaller, as well as 5% and 10% larger than the reference volume. The total energy of the unit cell was then determined for all these configurations, including the reference one. All the obtained energy–volume data points were fitted to the Murnaghan equation of state [20] to construct an approximating curve for the total energy as a function of the unit cell volume (and consequently, of a). The optimal value of a was determined from the minimum of this curve. Subsequently, to determine the internal free parameter δ (see Table 1), its value was varied iteratively, and the resultant force acting on the O1 atom was calculated at each step. The optimal value was considered to be the one at which the magnitude of the resultant force did not exceed 1 mRy/Bohr. The results are presented in Table 2.

Table 2. Calculated unit cell parameters for the $Ln_2Zr_2O_7$ (Ln = La, Nd, Sm, Eu, and Gd) compounds.

Compound	a, Å	δ	R_{mt}(Ln), Å	R_{mt}(Zr), Å	R_{mt}(O), Å
$La_2Zr_2O_7$	10.8790	0.3317	1.2594	1.106	1.00
$Nd_2Zr_2O_7$	10.7310	0.3353	1.2700	1.100	0.99
$Sm_2Zr_2O_7$	10.6825	0.3359	1.2647	1.095	0.99
$Eu_2Zr_2O_7$	10.5865	0.3376	1.2541	1.090	0.98
$Gd_2Zr_2O_7$	10.5804	0.3384	1.2341	1.090	0.98

In our calculations, the exchange-correlation functional in the PBE form without additional corrections was used during the lattice geometry optimization, as such corrections usually do not have a significant effect on it.

To illustrate the features of the electronic structure of the investigated compounds, the calculated total and partial densities of states for $Sm_2Zr_2O_7$ with different spin orientations (spin-up in Figure 2 and spin-down in Figure 3) are presented in Figures 2 and 3. The electronic structures of the other compounds are similar, and their differences from those shown in Figures 2 and 3 will be discussed below.

As can be seen in Figures 2 and 3, the s-states of the rare-earth element (located ~37 eV below the valence band maximum) exhibit an energy splitting between the spin-up and spin-down channels. This splitting is a manifestation of the Zeeman effect induced by the magnetic field generated by the Sm f-electrons. Such splitting is absent in $La_2Zr_2O_7$ because La lacks occupied f-states, and it becomes progressively more pronounced when transitioning from $Nd_2Zr_2O_7$ to $Sm_2Zr_2O_7$, $Eu_2Zr_2O_7$, and $Gd_2Zr_2O_7$, in full accordance with the increasing number of occupied f-states in this series of compounds. Notably, although free Eu and Gd atoms possess the same number (seven) of occupied f-states, our calculations indicate that the valence of Eu is close to Eu^{3+}; thus, the outer-shell electron configurations are $4f^6 5d^1 6s^2$ for Eu and $4f^7 5d^1 6s^2$ for Gd. Consequently, the number of f-electrons also increases in the transition from Eu to Gd. In addition to this splitting, as the nuclear charge of the rare-earth element increases, the binding energy of the s-states expectedly increases, causing the s-band to shift toward more negative energies. The

values of the splitting and shift for the s-bands of the investigated compounds are provided in Table 3.

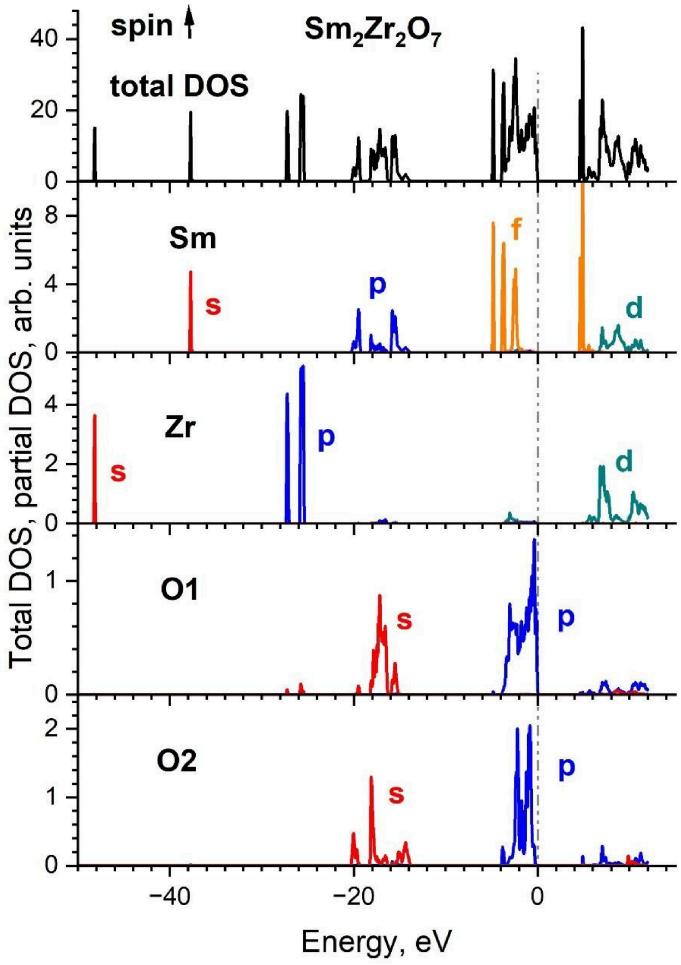


Figure 2. Total and partial densities of states for the spin-up channel in $Sm_2Zr_2O_7$.

Table 3. Splitting and shift of the Ln s-states (Ln = La, Nd, Sm, Eu, and Gd).

Compound	Splitting, eV	Shift, eV
$La_2Zr_2O_7$	0	0
$Nd_2Zr_2O_7$	0.24	−4.21
$Sm_2Zr_2O_7$	0.86	−6.93
$Eu_2Zr_2O_7$	1.28	−8.31
$Gd_2Zr_2O_7$	1.69	−10.08

The Sm p-band is situated approximately 16–20 eV below the valence band maximum. Similar to the s-band, it shifts toward more negative energies with increasing nuclear charge of the rare-earth element.

According to Hund's rule, it is energetically favorable to populate electron levels of the same symmetry (e.g., f-states) such that the spin orientation is preserved as long as possible. Consequently, as long as unoccupied f-states with a given spin direction (spin-up) remain, all f-states of the atom with the opposite spin (spin-down) remain empty. This is clearly evident in Figures 2 and 3. The majority of the spin-up Sm f-states are occupied and appear in Figure 2 below the Fermi level, a few electron volts below the valence band maximum, while the remaining states lie above the Fermi level at the very bottom of the conduction band. All Sm f-states with the opposite spin orientation (spin-down), shown in Figure 3,

are unoccupied and also contribute to the formation of the conduction band minimum. A similar scenario is observed for the other rare-earth elements, with the exceptions that La lacks occupied f-states (hence, all its f-states, both spin-up and spin-down, are located above the Fermi level) and that in Gd, all spin-up f-states are fully occupied.

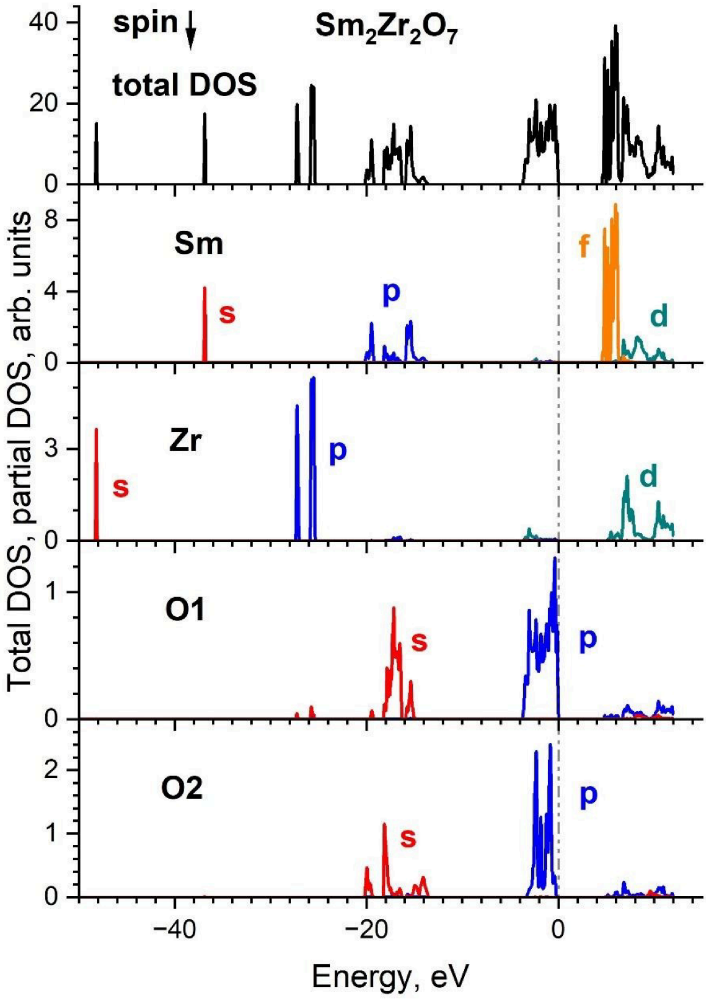


Figure 3. Total and partial densities of states for the spin-down channel in $Sm_2Zr_2O_7$.

The unoccupied d-states of Sm (and the other rare-earth elements) are situated near the bottom of the conduction band, slightly higher in energy than the f-states.

The energy positions of the Zr s-states and the p-states, which are split by spin–orbit coupling into $p^{1/2}$ and $p^{3/2}$ levels, remain practically unchanged across all investigated compounds (~48, 26.5, and 25.5 eV below the valence band maximum, respectively). The $4d^2$ electrons of the free Zr atom participate in chemical bonding within the studied compounds; consequently, d-states are practically absent from the Zr valence band (see Figures 2 and 3).

The s- and p-bands of the O1 and O2 oxygen atoms predictably shift slightly toward higher binding energies with increasing nuclear charge of the Ln atom, whereas the valence band maxima of all compounds are formed predominantly by oxygen p-states.

Figure 4 presents the real and imaginary parts of the dielectric function for the $Sm_2Zr_2O_7$ compound, calculated using the formulas for ε_2 (ω) and ε_1 (ω) from Ref. [21]. The overall shape and fine-structure features for the other pyrochlores are similar, taking into account the changes in their electronic structure described above.

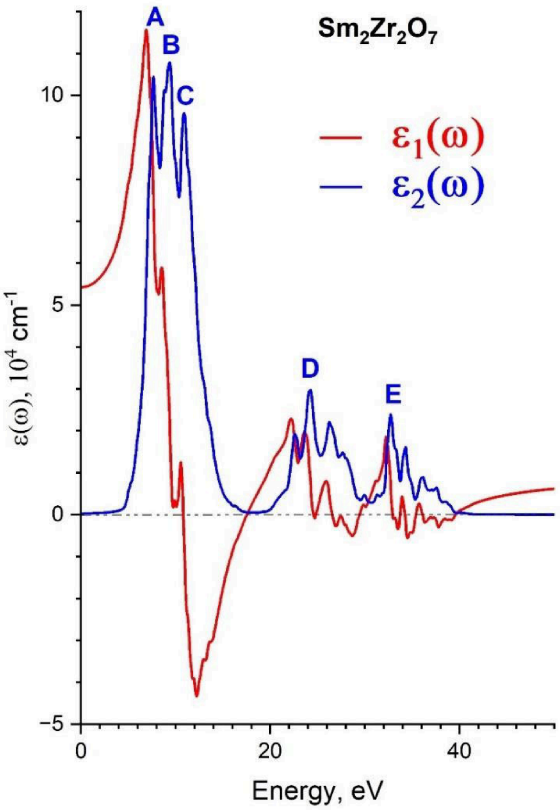


Figure 4. Real $\varepsilon_1(\omega)$ and imaginary $\varepsilon_2(\omega)$ parts of the dielectric permittivity tensor of $Sm_2Zr_2O_7$.

In the calculations of the imaginary part of the dielectric tensor, only dipole-allowed ($\Delta l = 1$) interband transitions were taken into account. Intraband electronic transitions are highly improbable and were not included in the present calculations. Within this framework, the peaks in the ε_2 (ω) curve (Figure 4) can be interpreted as follows: Peak A (7.66 eV)—transitions from the valence oxygen p-states to the unoccupied oxygen s-states; Peak B (9.37 eV)—transitions from the valence oxygen p-states to the unoccupied oxygen s-states, along with contributions from transitions from the occupied spin-up f-states to the unoccupied samarium (Sm) d-states; Peak C (10.9 eV)—transitions from the oxygen p- to oxygen s-states, and from the Sm f- to Sm d-states; the region near Peak D (24.26 eV)—transitions from the occupied oxygen s-states to the unoccupied oxygen p-states, combined with transitions from the occupied oxygen p-states to the unoccupied Sm d-states; the region near Peak E (32.72 eV)—transitions from the occupied p-states to the unoccupied Zr d-states.

Based on the real and imaginary parts of the dielectric permittivity tensor, the following optical properties of the investigated compounds were calculated:

1. Absorption coefficient, $\alpha(\omega)$;
2. Refractive index, $n(\omega)$;
3. Extinction coefficient, $k(\omega)$;
4. Reflection coefficient, $R(\omega)$;
5. Electron energy-loss spectrum, $L(\omega)$.

The calculated total densities of states (DOS) for all $Ln_2Zr_2O_7$ (Ln = La, Nd, Sm, Eu, and Gd) compounds, compared with their experimental X-ray photoelectron spectroscopy (XPS) spectra, are presented in Figure 5. The experimental XPS spectra were obtained by O.Yu. Khyzhun at the Institute for Problems of Materials Science of the National Academy of Sciences of Ukraine (Kyiv). A detailed description of the electron spectrometer and the experimental methodology is provided, for example, in Ref. [22].

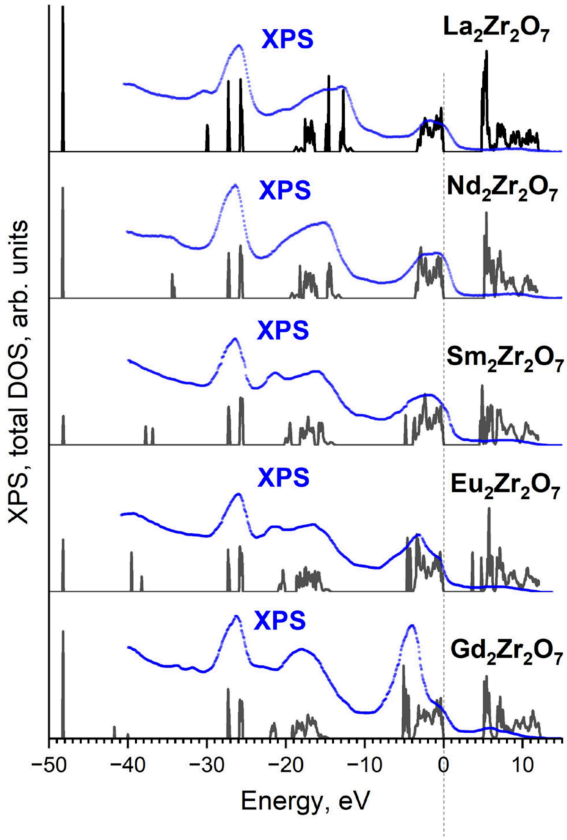


Figure 5. Total densities of states of $Ln_2Zr_2O_7$ (Ln = La, Nd, Sm, Eu, and Gd) in comparison with experimental X-ray photoelectron spectra (XPS).

In addition to the good agreement between the calculated values and the features of the experimental spectra, all the above-described trends regarding the splitting and the shift toward higher binding energies of the corresponding s- and p-states of the rare-earth elements are also clearly evident. The calculated band gap (E_g) values for all the investigated compounds are presented in Table 4.

Table 4. Band gap values for the $Ln_2Zr_2O_7$ compounds.

Compound	E_g, eV	
	Calculated	From Other Sources
$La_2Zr_2O_7$	4.818	3.52 [11], 4.1 [12]
$Nd_2Zr_2O_7$	5.160	2.67 [11], 4.0 [12]
$Sm_2Zr_2O_7$	4.579	2.86 [11], 4.7 [12]
$Eu_2Zr_2O_7$	3.566	4.6 [12]
$Gd_2Zr_2O_7$	4.770	4.2 [12]

Here, a clear trend is observed: the band gap (E_g) decreases as the spin-up f-band is progressively filled. The band gap reopens when no unoccupied spin-up f-states remain.

4. Conclusions

Based on quantum-mechanical calculations, a comparative analysis of the electronic structure of five zirconates with the pyrochlore structure was performed. The calculations confirm that the semiconducting state cannot be reproduced within the local density approximation (mean-field approximation). It is essential to account for the specific features of the 4f-electron interactions in the rare-earth elements (Nd, Sm, Eu, and Gd).

In all investigated compounds, the top of the valence band is formed by the 2p states of oxygen, the most electronegative element of the compounds. In the $Nd_2Zr_2O_7$, $Sm_2Zr_2O_7$, $Eu_2Zr_2O_7$, and $Gd_2Zr_2O_7$ compounds, the 4f states of the rare-earth element are located near the top of the valence band. Their energy position shifts from Nd to Gd towards higher binding energies.

The bottom of the conduction band is formed by the unoccupied 4f and 5d states of the rare-earth element and the 4d states of Zr.

The calculations reveal the splitting of the 5s-states of the rare-earth elements in the Ln = (Nd, Sm, Eu, and Gd) atoms induced by the magnetic field of the 4f-electrons.

The band gap decreases upon transitioning from Nd to Sm and further to Eu, owing to the increasing number of occupied 4f-electrons. When all spin-up (↑) 4f-states become fully occupied in Gd, the band gap (Eg) increases.

Author Contributions: Conceptualization, A.L.; methodology, B.G.; software, B.G., T.V.V. and K.K.; validation, B.G. and T.V.V.; formal analysis, B.G.; investigation, A.L., B.G. and T.V.V.; resources, T.V.V.; data curation, B.G.; writing—original draft preparation, T.V.V.; writing—review and editing, A.L. and T.V.V.; visualization, B.G. and T.V.V.; supervision, A.L.; project administration, A.L.; funding acquisition, A.L. All authors have read and agreed to the published version of the manuscript.

Funding: This research received no external funding.

Data Availability Statement: The original contributions presented in this study are included in the article. Further inquiries can be directed to the corresponding author.

Acknowledgments: During the preparation of this manuscript, the authors used LLM Qwen3.7-Plus for the purposes of text translation. The authors have reviewed and edited the output and take full responsibility for the content of this publication.

Conflicts of Interest: The authors declare no conflicts of interest.

Abbreviations

The following abbreviations are used in this manuscript:

APW	Augmented Plane Wave
APW + lo	Augmented Plane-Wave Plus Local Orbitals
DFT	Density Functional Theory
DOS	Density of States
GGA	Generalized Gradient Approximation
mBJ	Modified Becke–Johnson (potential)
PBE	Perdew–Burke–Ernzerhof (functional)
XPS	X-ray Photoelectron Spectrum

References

1. Stanek, C.R.; Minervini, L.; Grimes, R.W. Nonstoichiometry in $A_2B_2O_7$ Pyrochlores. *J. Am. Ceram. Soc.* **2002**, *85*, 2792–2798. [CrossRef]
2. Pirzada, M.; Grimes, R.W.; Minervini, L.; Maguire, J.F.; Sickafus, K.E. Oxygen Migration in $A_2B_2O_7$ Pyrochlores. *Solid State Ion.* **2001**, *140*, 201–208. [CrossRef]
3. Tabira, Y.; Withers, R.L.; Minervini, L.; Grimes, R.W. Systematic Structural Change in Selected Rare Earth Oxide Pyrochlores as Determined by Wide-Angle CBED and a Comparison with the Results of Atomistic Computer Simulation. *J. Solid State Chem.* **2000**, *153*, 16–25. [CrossRef]
4. Helean, K.B.; Ushakov, S.V.; Brown, C.E.; Navrotsky, A.; Lian, J.; Ewing, R.C. Formation Enthalpies of Rare Earth Titanate Pyrochlores. *J. Solid State Chem.* **2004**, *177*, 1852–1866. [CrossRef]
5. Lian, J.; Zu, X.T.; Kutty, K.V.G.; Chen, J.; Wang, L.M.; Ewing, R.C. Ion-Irradiation-Induced Amorphization of $La_2Zr_2O_7$ Pyrochlore. *Phys. Rev. B* **2002**, *66*, 054108. [CrossRef]

6. Chen, J.; Lian, J.; Wang, L.M.; Ewing, R.C.; Wang, R.G.; Pan, W. X-ray Photoelectron Spectroscopy Study of Disordering in $Gd_2(Ti_{1-x}Zr_x)_2O_7$ Pyrochlores. *Phys. Rev. Lett.* **2002**, *88*, 105901. [CrossRef] [PubMed]
7. Ewing, R.C.; Weber, W.J.; Lian, J. Nuclear Waste Disposal—Pyrochlore $A_2B_2O_7$: Nuclear Waste Form for the Immobilization of Plutonium and "Minor" Actinides. *Appl. Phys. Rev.* **2004**, *95*, 5949–5971. [CrossRef]
8. Vassen, R.; Cao, X.; Tietz, F. Zirconates as New Materials for Thermal Barrier Coatings. *J. Am. Ceram. Soc.* **2000**, *83*, 2023–2028. [CrossRef]
9. Chartier, A.; Meis, C.; Crocombette, J.; Corrales, L.R.; Weber, W.J. Atomistic Modeling of Displacement Cascades in $La_2Zr_2O_7$ Pyrochlore. *Phys. Rev. B* **2003**, *67*, 174102. [CrossRef]
10. Minervini, L.; Grimes, R.W. Disorder in Pyrochlore Oxides. *J. Am. Ceram. Soc.* **2000**, *83*, 1873–1878. [CrossRef]
11. Uno, M.; Kosuga, A.; Okui, M.; Horisaka, K.; Muta, H.; Kurosaki, K.; Yamanaka, S. Photoelectrochemical study of lanthanide zirconium oxides, $Ln_2Zr_2O_7$ (Ln = La, Ce, Nd and Sm). *J. Alloys Compd.* **2006**, *420*, 291–297. [CrossRef]
12. Feng, J.; Xiao, B.; Wan, C.L.; Qu, Z.X.; Huang, Z.C.; Chen, J.C.; Zhou, R.; Pan, W. Electronic Structure, Mechanical Properties and Thermal Conductivity of $Ln_2Zr_2O_7$ (Ln = La, Pr, Nd, Sm, Eu and Gd) Pyrochlore. *Acta Mater.* **2011**, *59*, 1742–1760. [CrossRef]
13. Lavrentyev, A.A.; Gabrelian, B.V.; Tuan, V.V.; Kalmykova, K.F. Ab Initio Calculations of the Electronic-Energy Structure and Optical Properties of Lanthanum and Neodymium Pyrozirconates. *Adv. Eng. Res.* **2025**, *25*, 129–141. [CrossRef]
14. Lavrentyev, A.A.; Gabrelian, B.V.; Tuan, V.V.; Kalmykova, K.F. Electronic Structure Characteristics of Complex Chalcogenides, Halides, and Oxides from Quantum-Mechanical Calculations. *Adv. Eng. Res.* **2026**, *26*, 2283. [CrossRef]
15. Blaha, P.; Schwarz, K.; Tran, F.; Laskowski, R.; Madsen, G.K.H.; Marks, L.D. WIEN2k: An APW+lo Program for Calculating the Properties of Solids. *J. Chem. Phys.* **2020**, *152*, 074101. [CrossRef] [PubMed]
16. Perdew, J.P.; Burke, K.; Ernzerhof, M. Generalized Gradient Approximation Made Simple. *Phys. Rev. Lett.* **1996**, *77*, 3865–3868. [CrossRef] [PubMed]
17. Tran, F.; Blaha, P. Accurate Band Gaps of Semiconductors and Insulators with a Semilocal Exchange-Correlation Potential. *Phys. Rev. Lett.* **2009**, *102*, 226401. [CrossRef] [PubMed]
18. Anisimov, V.I.; Solovyev, I.V.; Korotin, M.A.; Czyżyk, M.T.; Sawatzky, G.A. Density-Functional Theory and NiO Photoemission Spectra. *Phys. Rev. B* **1993**, *48*, 16929–16934. [CrossRef] [PubMed]
19. Pela, R.R.; Hsiao, C.-L.; Hultman, L.; Birch, J.; Gueorguiev, G.K. Electronic and optical properties of core–shell InAlN nanorods: A comparative study via LDA, LDA-1/2, mBJ, HSE06, G_0W_0 and BSE methods. *Phys. Chem. Chem. Phys.* **2024**, *26*, 7504–7514. [CrossRef] [PubMed]
20. Murnaghan, F.D. The Compressibility of Media under Extreme Pressures. *Proc. Natl. Acad. Sci. USA* **1944**, *30*, 244. [CrossRef] [PubMed]
21. Ambrosch-Draxl, C.; Sofo, J.O. Linear Optical Properties of Solids within the Full-Potential Linearized Augmented Planewave Method. *Comput. Phys. Commun.* **2006**, *175*, 1–14. [CrossRef]
22. Gabrelian, B.V.; Lavrentyev, A.A.; Vu, T.V.; Kalmykova, K.F.; Ananchenko, L.N.; Tkach, V.A.; Parasyuk, O.V.; Khyzhun, O.Y. Valence-Band Electronic Structure and Main Optical Properties of $Cu_2HgGeTe_4$: Theoretical Simulation within a DFT Framework and Experimental XPS Study. *Mater. Today Commun.* **2020**, *23*, 100828. [CrossRef]

Disclaimer/Publisher's Note: The statements, opinions and data contained in all publications are solely those of the individual author(s) and contributor(s) and not of MDPI and/or the editor(s). MDPI and/or the editor(s) disclaim responsibility for any injury to people or property resulting from any ideas, methods, instructions or products referred to in the content.